



Hybrid functionals with nonempirical Hartree-Fock parameters for electronic structure calculation of layered oxides

Konstantin Köster  and Payam Kaghazchi *

*Institute of Energy and Climate Research, IEK-1 Materials Synthesis and Processing,
Forschungszentrum Jülich GmbH, 52425 Jülich, Germany*

MESA+ Institute for Nanotechnology, University of Twente, Enschede 7500 AE, The Netherlands



(Received 26 January 2024; revised 14 March 2024; accepted 20 March 2024; published 11 April 2024)

Accurate electronic structure descriptions of layered oxides are highly relevant yet complex to obtain by *ab initio* methods. The functionalities of layered transition metal oxides are usually heavily influenced by their electronic structure and the hybridization/delocalization of *d* electrons of the transition metals. Therefore understanding the electronic structure can enable a more rational design of this highly important material class, which is widely utilized in practical applications such as cathodes in secondary batteries of portable electronic devices and electric vehicles. However, it is well known that standard quantum-mechanic approximations to the many-body problem overlocalize (Hartree-Fock) or overdelocalize (density functional theory) electrons in these systems. A mixture of different methods (hybrid functionals) can partially resolve the problem but introduces at least one additional parameter (the mixing parameter) that has to be determined by e.g., higher levels of theory (*GW*). In this study, we focus on the electronic structure of lithiated layered transition-metal oxides based on Co, Ni, Mn, and their binary systems that form the foundation of state-of-the-art lithium-ion batteries. The influence of Hartree-Fock mixing in the PBE0 hybrid functional on the electronic structure is compared as well as using different Hartree-Fock mixings as starting points for *GW* calculations. Two nonempirical *GW*-based fitting approaches to determine the optimal Hartree-Fock mixing are considered. We show that one of the fitting approaches suggests small mixing parameters and is in satisfactory agreement with experimental results, while the other approach has a stronger theoretical foundation and indicates higher mixing parameters, which are close to the value obtained by perturbation theory by Perdew, Ernzerhof, and Burke. Finally, it is shown that larger mixing parameters are required when screening is introduced to the Hartree-Fock term.

DOI: [10.1103/PhysRevB.109.155134](https://doi.org/10.1103/PhysRevB.109.155134)

I. INTRODUCTION

Transition metal (TM) oxides are very important materials due to their broad applicability in multiple fields, but it is challenging to describe their electronic structures correctly by *ab initio* methods [1–6]. Among the different classes of TM oxides, layered ones with the composition $A[\text{TM}]\text{O}_2$ are among the most appealing. They are already utilized as cathodes in state-of-the-art energy storage devices and are modified to meet the needs of next generation of energy-storage materials [7,8]. In these materials, alkali metals (A) are reversibly intercalated and deintercalated as charge carriers between the cathode and the anode while the electrons are moving through an external circuit, allowing to obtain the stored electrical energy from these materials. In particular, layered oxide cathode materials based on Co, Mn, and Ni along with Li as charge carrier have become the market standard for energy storage and are employed in multiple devices nowadays [7]. LiCoO_2 was first proposed by Goodenough in Ref. [9] in 1980 and became later the first commercialized secondary Li-ion battery by Sony Corp. [10]. The LiNiO_2 [11] and LiMnO_2 [12] materials were first introduced a few years later as cathode active

materials for lithium ion batteries. Nowadays, cathodes with different mixtures of these TMs are most frequently employed in high-performance batteries where Mn can also be replaced by Al [7]. For practical use cases — not limited to the field of batteries — the correct description of the electronic structure is especially important as it determines some of the key properties of TM oxides (e.g., band gap, redox process) but is hard to come by with computational methods. This yields to some controversies for the calculation of redox processes in these materials [13–15].

Standard methods such as Hartree-Fock (HF) or density functional theory (DFT) with a generalized-gradient-approach (GGA) based exchange-correlation (xc) functional fail to accurately predict the electronic structures of TM oxides as they over-localize or over-delocalize the electrons onto the ion cores due to their well-known intrinsic errors (missing correlation in HF and self-interaction errors in DFT) [16]. This yields an inadequate description of the *d* electrons that are of special importance for the aforementioned practical applications of these materials [17–19]. Using the band gap as an indicator for the correct description of electronic structure, it can be shown that HF tends to overestimate, whereas DFT-GGA tends to underestimate the band gaps compared to experimental studies [20]. As both approaches seem to be complementary to some extent, it was proposed to mix a

*p.kaghazchi@fz-juelich.de

portion of exact exchange (HF) with the exchange of DFT to improve the accuracy with the cost of increased computational effort [21]. This approach is known as hybrid-functional and its superiority over the two bare methods for electronic structures is widely accepted [22–26]. It is also worth noting that another, computationally less demanding method, the Hubbard U (DFT+ U) method is commonly applied to describe TM oxides [1,27–30]. In a simplified picture this model applies a species-specific bias potential of the strength U , which localizes the electrons by introducing a penalty for partial occupations [31]. Hybrid functionals provide a more general treatment of the self-interaction error in DFT by avoiding species-specific auxiliary parameters and the risk of perturbing the electronic structure [14,23,28]. We will focus on hybrid functionals in this work, especially the one-parameter formulation proposed by Becke in Ref. [32]: PBE0 (also sometimes called PBEh), which is described by the following formula:

$$E^{\text{PBE0}} = \alpha \times E_x^{\text{HF}} + (1 - \alpha) \times E_x^{\text{PBE}} + E_c^{\text{PBE}}. \quad (1)$$

The value of α (HF mixing parameter) is usually set to 25% which can be reasoned by perturbation theory [33]. However, $\alpha = \frac{1}{2}; \frac{1}{3}; \frac{1}{4}; \frac{1}{5}$ can all be reasoned by pure theory approaches (Ref. [34]) and it is also widely accepted to fit the parameter to experimental and/or theoretical benchmarks [6,35–38]. Moreover, position-dependent local mixing parameters are also employed that allow to vary the effective mixing spatially with respect to the different ion-species [22,39]. Regarding the nonlocal hybrid functional approach, it should also be noted that more complex, screened approaches exist (e.g., HSE [40,41]) that split the exchange in a long range (LR) and a short range (SR) to apply a screening to the Hartree-Fock exchange. To reduce the computational demand, this method considers only the SR Hartree-Fock exchange [cf. Eq. (2)] introducing another parameter, the screening parameter ω , that can be freely optimized [40,41]

$$E^{\text{HSE}} = \alpha \times E_{x,\text{HF}}^{\text{SR}} + (1 - \alpha) \times E_{x,\text{PBE}}^{\text{SR}} + E_{x,\text{PBE}}^{\text{LR}} + E_c^{\text{PBE}}. \quad (2)$$

It should be mentioned that also physically motivated approaches were developed to determine HF mixing/range separation in hybrid functionals such as dielectric-dependent hybrid functionals [42], optimally tuned hybrid functionals (ionization potential theorem) [43,44], and hybrid functionals aimed to satisfy Koopman’s condition [45]. In all these hybrid functionals, the HF mixing has a significant influence on several electronic properties calculated for the material under study [6,46,47]. A correct description of electronic structure is essential for layered TM oxides as cathode materials since it determines the redox process, especially the activity of oxygen redox in the compound [15,48,49]. To further rationalize the design of novel layered TM oxide cathode materials by computational methods accurate electronic structures are required that can be effectively tuned by varying the HF mixing in hybrids.

As mentioned above, one strategy is to fit the HF mixing to calculated reference electronic structures by higher levels of theory for example within the so-called GW approximation: The first term in the expansion of the self-energy in the

Green’s function G and the dynamically screened Coulomb interaction W , obtained within the random phase approximation [50,51]. This approach has already been proven to be practical for obtaining reference electronic structures and fitting HF mixing by several other studies [6,38,52]. In the GW approximation quasiparticle energies E_{nk}^{QP} are given by [53]

$$E_{nk}^{\text{QP}} = \text{Re}[\langle \psi_{nk} | T + V_{n-e} + V_H + \Sigma(E_{nk}^{\text{QP}}) | \psi_{nk} \rangle]. \quad (3)$$

Band and k -point indices are denoted as n and \mathbf{k} , T is the kinetic-energy operator, V_{n-e} and V_H are the nuclei and Hartree potential, respectively. The self-energy operator Σ is constructed from G and W as mentioned before. The quasiparticle energies are then updated by adding Eq. (3), scaled by a renormalization factor, to the quasiparticle energies of the previous cycle. Naturally, this *ansatz* requires a starting point for the quasiparticle energies which is commonly obtained by DFT calculations [54–56]. In the single-shot GW method (G_0W_0), Eq. (3) is only evaluated once (and so the self-energy) and added to the starting point. In contrast, in the fully self-consistent GW approach (GW) the procedure is iterated to convergence by updating the single electron energies in Σ along with reconstructing W based on the most recent quasiparticle energies. There is also the possibility to fix W during these iterations for the partially self-consistent GW (GW_0) approach. It should be noted that for all GW calculations in this work off-diagonal elements of the self-energy were considered to be equal to the corresponding elements of the DFT exchange-correlation potential, which is only justified if the wave functions of the starting point are in sufficient agreement with the ones of GW [51]. This kind of GW is sometimes also denoted as “ev GW ”.

Even though the GW approach has a strong theoretical foundation, the critical point is still to select an appropriate DFT starting point. Higher levels of GW can reduce the starting-point dependence, but the results of all levels still depend on the starting wave functions and band gaps can vary strongly by starting point and level of GW [57]. It was suggested to employ G_0W_0 starting from hybrid functionals and GW_0 on top of DFT-GGA calculations, while GW is shown to tend to overestimate band gaps, regardless of the starting point [51,58]. Consequently, it seems valuable to also scan the results of GW at intermediate starting points as DFT-GGA can be tuned by adding HF mixing step-wise towards the default value of 25% for hybrids, as it was already investigated by Chen *et al.* [38] for some semiconductors and insulators.

In this work, we adopt the band gap as the key property to optimize the electronic-structure calculations using hybrid functionals by adjusting the HF mixing-parameter. Prototype layered oxides of Co, Mn, and Ni and their binary mixtures are investigated at their fully lithiated state, since previous works suggested the largest adjustment to the default mixing parameter at high lithium contents [6]. Band gaps at various HF mixings are calculated in the PBE0 approach and G_0W_0 calculations are employed to each PBE0 solution. Two optimal sets of mixing parameters for PBE0 are found for the materials under study and the corresponding band gaps are compared to experimental values. Moreover, the influence of

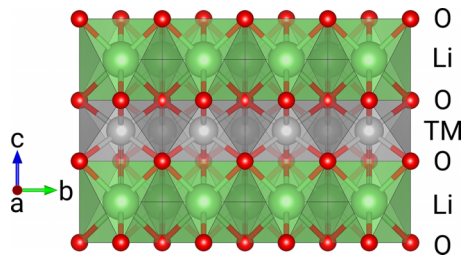


FIG. 1. Exemplary structure of the models employed in this study showing the transition metals (TM) in silver in an octahedral coordination as well as the lithium ions in green also in octahedral coordination along with the red oxygen layers.

using a screened hybrid and higher levels of *GW* on band gaps and optimal HF mixing parameters is discussed.

II. METHOD

All calculations were carried out using the projector augmented wave (PAW) method [59] as implemented in the Vienna *ab initio* simulation package (VASP) [60]. Pseudopotentials optimized for *GW* calculations that explicitly describe outer *s* (Li), *s* and *p* (O), and *s* and *d*-electrons (TM) were employed, while *d* projectors were considered for the oxide ions. The spin-polarized calculations were performed with a $4 \times 2 \times 4$ *k*-point grid including the Γ point along with an energy cutoff of 600 eV. Nonspherical contributions from the gradient corrections were accounted for in all calculations. Furthermore, partial occupancies were treated with Gaussian smearing along with a smearing width of 0.01 eV. Density of states (DOS) was calculated with the tetrahedron method. Layered oxides of LiCoO_2 , LiNiO_2 , LiMnO_2 , $\text{LiCo}_{0.5}\text{Mn}_{0.5}\text{O}_2$, $\text{LiCo}_{0.5}\text{Ni}_{0.5}\text{O}_2$, and $\text{LiMn}_{0.5}\text{Ni}_{0.5}\text{O}_2$ were modeled by $1 \times 3 \times 1$ supercells containing six formula units and in the $C2/m$ space-group (O1 phase) as shown in the exemplary model in Fig. 1.

It should be noted that the experimentally observed $\text{Li}_{1-x}\text{Ni}_{1+x}\text{O}_2$ defects (nonstoichiometric compositions) [61] for LiNiO_2 were not accounted for in our model for the sake of simplicity. Moreover, LiCoO_2 , which generally has been observed to have a $R\bar{3}m$ space group (O3 phase according to the notation for layered TM oxides by Delmas *et al.* [62]), has been modelled by a O1 structure. We carefully checked that both space groups yield essentially the same band gaps at various levels of theory. However, it should be mentioned that other layered TM oxides show a weak space group dependence of band gap [63].

The overall calculation process can be structured into three steps: geometry optimization (a), electronic structure optimization (b), and *GW* calculations (c).

A. Geometry optimization

Geometries of all symmetry-distinctive TM arrangements were fully optimized for each compound without symmetry constrains using the generalized-gradient-approach (GGA) within the Perdew-Burke-Ernzerhof (PBE) exchange-correlation functional [64]. An electronic convergence criterion of 10^{-8} eV was employed and the geometry was

optimized until the forces of each ion were lower than 10^{-3} eV/Å. The total energy of the structures was found to be reasonably converged (<0.0025 eV per formula unit) with respect to *k*-points and cutoff energy. The optimized geometry of the lowest energy structure for each compound was fixed for the following calculation steps.

B. Electronic structure optimization

Different ferro-magnetic (FM) and anti-ferro-magnetic (AFM) arrangements in the compounds containing magnetic ions were tested on the PBE level to identify the most favorable magnetic configurations. Using the PBE geometries and magnetic structures, electronic structures were optimized within the single-parameter PBE0 hybrid-functional approach [32] varying the Hartree-Fock mixing parameter. Same settings were applied for screened hybrid functional calculations [65]. A convergence criterion of 10^{-8} eV was employed and the “Accurate” setting of VASP was used for the DFT part of the calculations. In a consecutive step, an exact diagonalization of the Hamiltonian was performed while the number of bands was increased to 256 resulting in more than 150 unoccupied bands for all investigated compounds.

C. *GW* calculations

Single-shot *GW* calculations considering just eigenvalues (G_0W_0 calculations) were performed for all compounds to obtain the quasiparticle energies. However, for LiCoO_2 and LiNiO_2 , *G* and *W* were also both iterated to convergence to obtain fully self-consistent (in eigenvalues) *GW* results (denoted “*GW*” in this work but in other works sometimes also referred to as “*evGW*”). The iterations were stopped when the band gap was converged within at least 0.1 eV. For *GW* calculations, the energy cutoff for the response function was set to 400 eV and the number of frequency/time grid points was set to 100. Quasiparticle energies were calculated for all bands that lie within twice the number of occupied states. Convergence tests with higher cutoffs, more grid points, more bands, and calculating quasiparticle energies for more unoccupied bands showed that the band gap is well converged ($\ll 0.1$ eV) with the chosen settings.

Atomistic structures and isosurfaces were visualized with help of the VESTA software-package [66] and charge density differences were calculated with the help of VASPKIT [67].

III. RESULTS AND DISCUSSION

A. DFT optimizations and influence of different portions of HF mixing within the PBE0 functional

The optimized geometries revealed an intermediate Jahn-Teller distortion for LiNiO_2 and a strong Jahn-Teller distortion for LiMnO_2 , whereas LiCoO_2 showed an almost perfect symmetrical coordination (cf. Fig. 3). These geometries are in agreement with previous studies and experimental observations as well as with the general Jahn-Teller activity of *d*-configurations assuming charges of 3+ for the TM ions [68]. Distortions were, however, much weaker in the mixed materials ($\text{LiCo}_{0.5}\text{Mn}_{0.5}\text{O}_2$, $\text{LiCo}_{0.5}\text{Ni}_{0.5}\text{O}_2$, and $\text{LiMn}_{0.5}\text{Ni}_{0.5}\text{O}_2$) and not present around Co. Only Ni in

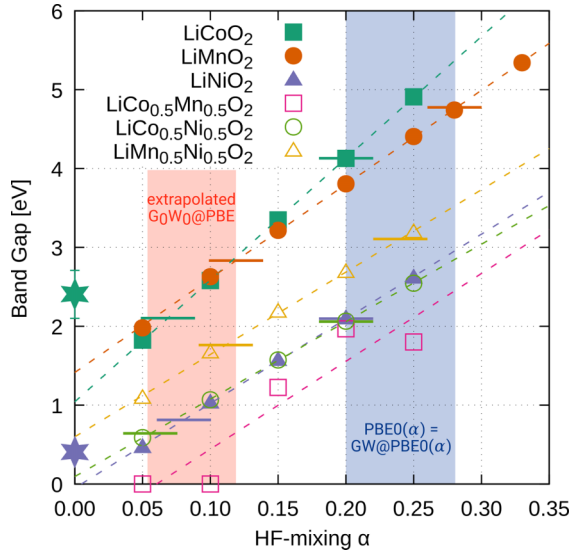


FIG. 2. PBE0 band gaps of the investigated layered TM oxides as a function of the HF mixing-parameter α . The band gaps increase linearly with α as indicated by the linear fits (dashed lines). Horizontal solid bars in the α range marked red (left) correspond to the optimal mixing parameters to reproduce the extrapolated $G_0W_0@PBE$ band gaps. The horizontal bars in the α range marked in blue (right) show the mixing parameters that result in no correction of the band gap in consecutive GW calculations. Stars on y axis mark experimental band gaps as shown in Table I.

$\text{LiCo}_{0.5}\text{Ni}_{0.5}\text{O}_2$ showed a significantly distorted environment. Regarding the magnetic ordering, our calculations indicated no magnetism (unpaired electrons) for LiCoO_2 , FM ordering for LiNiO_2 and $\text{LiCo}_{0.5}\text{Ni}_{0.5}\text{O}_2$, and AFM ordering was found to be most favorable for LiMnO_2 and $\text{LiMn}_{0.5}\text{Ni}_{0.5}\text{O}_2$. Moreover, a high-spin configuration was obtained for Mn in LiMnO_2 which is in agreement with the literature where also an AFM high-spin configuration is reported for LiMnO_2 [69]. Using these models to optimize electronic structures, we find that band gap increases linearly with the HF mixing-parameter (α) of PBE0 (Fig. 2 and fitted parameters in Table II). The linear trend agrees with previous studies on various materials [6,70–72].

Only for $\text{LiCo}_{0.5}\text{Mn}_{0.5}\text{O}_2$ no linear trend is observed as the electronic structure undergoes significant changes with α , which is concluded from the computed unpaired electrons (UPE) on Co and Mn (Table III for $\alpha = 25\%$): In the α range from 0% to 10% three $\text{Co}^{2.67+}$ and three $\text{Mn}^{3.33+}$ can be assigned with the partial charges being delocalized over all ions of the same type. For α between 15% and 20% three Co^{3+} and three Mn^{3+} are observed and for $\alpha = 25\%$ two Co^{3+} , one Co^{2+} , two Mn^{3+} , and one Mn^{4+} are obtained in the electronic structure corresponding to the same average charges as for the α range from 0% to 10% but with the partial charges in the average being fully localized on single ions. These changes of the electronic structure with α and changes on how electrons are localized/delocalized between/within the two different metal species become problematic when comparing electronic structures of two different α for $\text{LiCo}_{0.5}\text{Mn}_{0.5}\text{O}_2$. The reason for this behavior might be found in electron affinity (e.g., estimated by electronegativity) as the one of Co is closer to that of

Mn compared to Ni-Mn, which presumably causes intermediate degree of reduction of Co in favor of oxidation of Mn with roughly 1/3 of the Co being reduced to 2+ and 1/3 of the Mn being oxidized to 4+. In contrast, the electron affinities of Co and Ni are more similar resulting in 3+ ions for both species in $\text{LiCo}_{0.5}\text{Ni}_{0.5}\text{O}_2$ and those of Ni and Mn are more different resulting in full oxidation of Mn to Mn^{4+} and reduction of Ni to Ni^{2+} in $\text{LiMn}_{0.5}\text{Ni}_{0.5}\text{O}_2$ which can be again verified by UPE in the electronic structures (cf. Table III). Varying α in these compounds changes localization/delocalization of electrons for each transition-metal ion but does not result in different localizations of oxidations between or within the ionic species. Consequently, electronic structures at different α are comparable for all materials but $\text{LiCo}_{0.5}\text{Mn}_{0.5}\text{O}_2$.

These oxidation states also agree with the missing Jahn-Teller distortion in $\text{LiMn}_{0.5}\text{Ni}_{0.5}\text{O}_2$ as both ions are not Jahn-Teller active in these charge states in contrast to their 3+ ions. In general, the results indicate that a critical range of difference in electron affinity exists. In this range delocalizations of electrons over the TMs can appear. At smaller differences in electron affinity, both species show the same oxidation state and at larger differences one species is fully oxidized and the other fully reduced. Therefore it becomes evident that the anomalous lower electronegativity of Mn compared to Co and Ni is the main challenge in predicting the correct electronic structure for mixtures comprising of Mn, Ni, and/or Co. As mentioned above, the dependence of α on localization/delocalization of partial charges between Co and Mn for $\text{LiCo}_{0.5}\text{Mn}_{0.5}\text{O}_2$ prevents a fair comparison of electronic structures at different α for this composition. By applying an effective Hubbard correction of 5 eV to both Mn and Co, the localized charge states that were obtained in the calculations with 25% HF mixing were successfully stabilized for the smaller mixing parameters. However, the calculated electronic structures were in a high-spin and not a low-spin configuration that was observed in the Hubbard-free calculations at $\alpha = 25\%$. This complex behavior of a simple binary system shows that first, a carefully chosen α , for example by fitting to some additional input, is required and second, that a description via adjustment of α is desirable over correction by a bias potential (e.g., Hubbard). It is to expect that this effect becomes more severe in more practical ternary or quaternary systems underlining the importance of tuning α in the employed computational methods for layered TM oxides.

The aforementioned linear trend of increasing band gap with the HF mixing-parameter for the other materials except $\text{LiCo}_{0.5}\text{Mn}_{0.5}\text{O}_2$ can be explained by the tendency of over-localization of HF and over-delocalization of DFT-GGA. Adding more of the over-localized part widens the band gap by diminishing electron density between the ions. This trend is visualized by the charge-density-difference (CDD) plots in Fig. 3 showing the computed CDD for LiCoO_2 , LiMnO_2 , and LiNiO_2 at various HF mixing-parameters with respect to PBE.

The CDD plots show a depletion of electrons around the TM ions that is centered along the TM-O bonds and for LiCoO_2 and LiNiO_2 also a small accumulation between the TM-O bonds. The shapes of these depletions are in agreement with Jahn-Teller distortions in LiNiO_2 and LiMnO_2 as LiMnO_2 shows no depletion along the elongated axis of

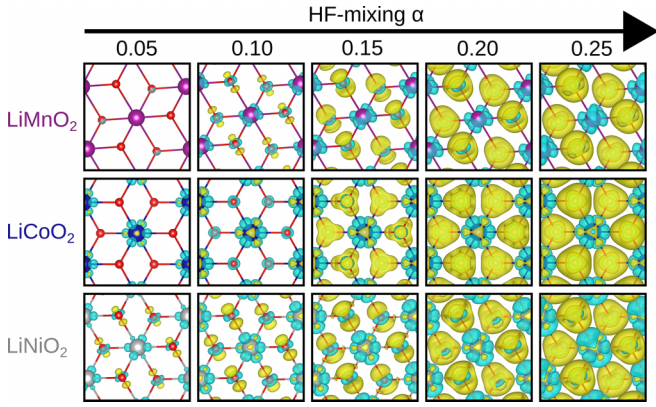


FIG. 3. Charge density differences (CDDs) of LiMnO₂, LiCoO₂, LiNiO₂ (from top to bottom) at different HF mixing-parameters ranging from 5% to 25% (from left to right) relative to their PBE density (HF mixing of zero). All iso-surfaces are shown at an isovalue of 2.5×10^{-3} electrons/Å³, while electron accumulation is indicated by yellow color and electron depletion by turquoise color.

the coordination octahedron, while LiNiO₂ shows a spatially expanded depletion along the elongated axis. In general, differences become stronger at higher mixing parameters and are relatively similar for LiCoO₂ and LiNiO₂ (despite the Jahn-Teller distortion in LiNiO₂), while weaker for LiMnO₂. Although the computed CDD on TMs coincides with the picture of localizing the electrons stronger onto the ion cores by adding more HF mixing, the CDD on oxygens shows the opposite trend: an electron depletion is observed on O anions which increases with α . However, a significant accumulation of electrons along the O-TM bonds from oxygen is also observed for $\alpha = 0.15, 0.20,$ and 0.25 , distributing more homogeneously around O-TM bonds at higher HF mixings. This indicates delocalization of oxygen electrons. These results outline the holistic approach of changing HF mixing to tune the electronic structure rather than using more local corrections. However, it must be noted that the shown changes in CDD are overall small but allow for qualitative statements about trends in localization/delocalization.

To further comment on the hybridization of O 2*p* and TM 3*d* orbitals, we defined a degree of hybridization η as described in Eq. (4) by integrating the projected densities of states (pDOS). Consequently, η can take values between 0 and 1 where 1 is maximal hybridization ($\text{pDOS}_{\text{O}2p} = \text{pDOS}_{\text{TM}3d}$) and 0 indicates no overlap of the different pDOS (no hybridization).

$$\eta = 1 - \frac{\int_a^b |\text{pDOS}_{\text{O}2p} - \text{pDOS}_{\text{TM}3d}| dE}{\int_a^b \text{pDOS}_{\text{O}2p} dE + \int_a^b \text{pDOS}_{\text{TM}3d} dE}. \quad (4)$$

It can be assumed that the high energy states are most important for hybridization and therefore the energy range was set to $a = -2$ to $b = 0$ eV where 0 eV corresponds to the Fermi level. A similar hybridization measurement in the same energy range was also employed by Seo *et al.* [6] for LiCoO₂, allowing for comparison to their study. As spin-polarized calculations were performed, both, spin-up and spin-down pDOS were considered separately and added to plot the degree of hybridization versus the HF mixing-parameter in Fig. 4.

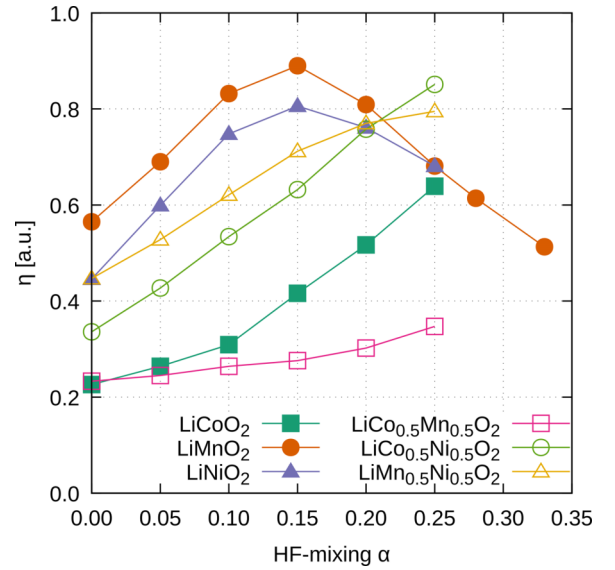


FIG. 4. Dependency of the degree of hybridization η of O 2*p* and TM 3*d* orbitals as defined in Eq. (4) on the HF mixing-parameter α for the different layered TM oxides under investigation.

Hybridization in LiCoO₂ increases almost exponentially with the HF mixing in Fig. 4 which is in agreement to the aforementioned study by Seo *et al.* [6]. Generally, different trends can be observed for the materials varying from a linear increase of hybridization with α (e.g., LiCo_{0.5}Ni_{0.5}O₂) to a parabola shape with a maximum in hybridization at a HF mixing of 15% (e.g., LiMnO₂ and LiNiO₂). The hybridization trend in Fig. 4 is mainly governed by the change in the intensity of the TM and O pDOS plots in Fig. 6. The TM pDOS for LiCoO₂ has the strongest intensity right below the Fermi level and the intensities of the O pDOS become closer to TM pDOS at higher HF mixing but never reach the TM pDOS intensities. LiMnO₂ shows the same trend but at 15% HF-mixing both pDOS are almost the same and at higher mixing the intensities of the O pDOS exceeding the TM pDOS. These behaviors result in the trends observed in the hybridization plot in Fig. 4. It could be argued that the *d*-orbital splitting influences which *d* orbitals are located directly below the Fermi level and are therefore available for a hybridization with O 2*p* orbitals. As a consequence, the strongly Jahn-Teller distorted materials (LiMnO₂ and LiNiO₂) show a more different behavior of hybridization and HF mixing because of their electronic configuration.

B. Single-shot GW band gaps at different PBE0 HF mixing and optimal HF mixing-parameters

Having shown that variation of the HF-mixing parameters has an significant influence on certain important properties such as band gap and hybridization we proceeded to perform G_0W_0 calculations to identify the most suitable HF mixing-parameter. Consecutive G_0W_0 calculations were performed on top of all the PBE0 calculations at different HF mixings discussed in the previous section. This procedure allows to consider and analyze the strong starting-point dependence of

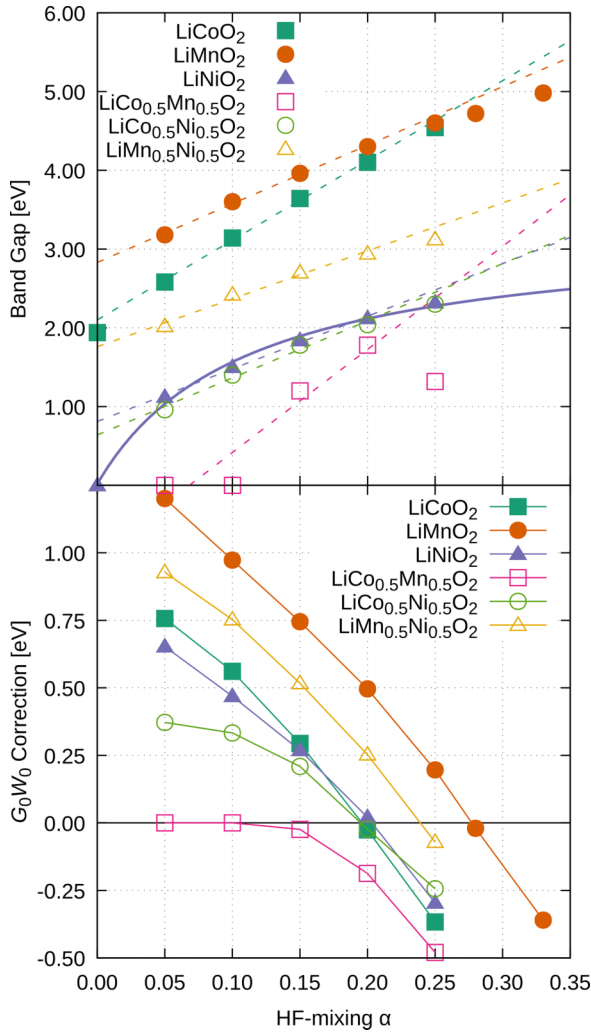


FIG. 5. The upper plot shows G_0W_0 band gaps as function of the HF mixing-parameter α in the PBE0 starting point. Linear fits for the values in the α range 5%–20% are shown by dashed lines and for LiNiO_2 also a fit of an inverse function that describes the whole α range seemingly well is plotted by a solid line. The lower plot shows the corrections G_0W_0 made to the band gap of the PBE0 starting point.

G_0W_0 calculations. The band gaps obtained from these calculations are shown in the upper plot of Fig. 5.

In general, the G_0W_0 band gaps maintain the rising trend of the underlying starting point with higher mixing parameters α but a perfect linear increase in band gaps with the HF mixing as observed for the PBE0 calculations (cf. Fig. 2) is not obtained. The consecutive G_0W_0 step shows no linearity at higher HF mixings (e.g., LiMnO_2) as well as low HF mixings (e.g., LiNiO_2). The latter trend is particularly pronounced for TM oxides which change their class by adding a small portion of HF mixing from metal (have no band gap) to insulator (have band gap) as shown by the nonlinear fit for LiNiO_2 in Fig. 5, upper plot. It should be also noted that the irregular behavior of the band gap of $\text{LiCo}_{0.5}\text{Mn}_{0.5}\text{O}_2$ due to the aforementioned changes in electronic structure with α is also present in the G_0W_0 calculations.

For intermediate α (5%–20%) the trend of the band gaps is reasonably approximated by a linear function indicated by the linear fits (dashed lines in Figure 5, upper plot) except for $\text{LiCo}_{0.5}\text{Mn}_{0.5}\text{O}_2$ due to the aforementioned irregular behavior of the electronic structure with α . Despite this trend it is still unclear what HF mixing acts as the most accurate starting point for G_0W_0 calculations for the layered TM oxides under study.

The linear (band gap versus α) functions fitted (cf. upper Fig. 5 and Table IV) for the 5% to 20% α range allow to extrapolate to a G_0W_0 @PBE solution. This extrapolation is particularly useful for compositions undergoing a change from metal to insulator by admixing HF (e.g., LiNiO_2). In that case PBE has no band gap and is therefore a unsuitable starting point that is far off the more linear trend observed at higher HF mixing-parameters. This might be because of an incorrect alignment of states in the starting point and/or a larger difference of the starting point wave functions to the GW wave functions. For LiCoO_2 , this extrapolated G_0W_0 @PBE band gap is only slightly higher (less than 0.2 eV) than the band gap calculated from the “real” PBE starting point. A pure PBE starting point is already quite suitable for LiCoO_2 because it predicts the metal-insulator properties correctly. However, for LiNiO_2 , where pure PBE predicts a metal, the extrapolated band gap increases more drastically. The proposed extrapolation method is intrinsically *ab initio* based as no experimental inputs are required. It should be noted that neither the linear fit nor the extrapolation approach have an physical meaning but employing these strategies seems to offer the best compromise between under- and overprediction of band gaps compared to experimental values, especially for LiCoO_2 and LiNiO_2 for which most experimental values exist.

For LiCoO_2 , the extrapolated G_0W_0 @PBE band gap of 2.10 eV perfectly matches the band gap of a very recent experimental study that determined a band gap of 2.15 eV [73] and another experimental value of 2.10 eV [74] (the experimental structures were O3 but it was checked that our calculations of the O1 structures for LiCoO_2 do not change significantly by using O3). Despite this excellent agreement with the experiments it is also worth noting that experimental band gap studies show quite some deviations and even a value of 2.7 eV [75] has been reported such that our calculated value is at the lower edge of experimental band gaps. For LiNiO_2 , the experimental studies are more sparse but one study suggested a band gap of 0.40 eV [27] which is significantly lower compared to the extrapolated G_0W_0 @PBE band gap of 0.81 eV. However, deviations would be even worse by using a starting point with (higher) HF mixing and also a pure PBE starting point would show almost the same deviation but in a different direction (under-prediction) and predicts metallic instead of insulator properties. For LiMnO_2 , some theory works exist that predict various band gap values, depending on structure, magnetism, and computational approach, about 1 eV lower compared to the extrapolated G_0W_0 @PBE band gap [76,77]. As our LiMnO_2 model considered a strong Jahn-Teller distortion along with AFM ordering which are both known to increase the band gap, it is also expected that the band gap of this material is comparably high. No final conclusion about its accuracy in the extrapolated G_0W_0 @PBE approach can be made for LiMnO_2 .

TABLE I. Optimal PBE0 HF mixing-parameters determined by extrapolated $G_0W_0@PBE$ ($\alpha^{\text{ext.}}$) and the PBE0 HF mixing-parameter that directly leads to the fully self-consistent GW band gaps (α^{GW}). Band gaps (BG) corresponding to the determined α are given along with experimental band gaps, where available. No values for $\text{LiCo}_{0.5}\text{Mn}_{0.5}\text{O}_2$ are given as the changes in the electronic structure with α prevented to apply any fitting approach.

Compound	$\alpha^{\text{ext.}}$ (%)	BG ^{ext.} (eV)	α^{GW} (%)	BG ^{GW} (eV)	BG ^{exp.} (eV)
LiCoO ₂	6.7	2.10	20	4.13	2.10 [74], 2.15 [73], 2.70 [75]
LiMnO ₂	11	2.83	28	4.77	—
LiNiO ₂	8.0	0.81	20	2.09	0.40 [27]
LiCo _{0.5} Mn _{0.5} O ₂	—	—	—	—	—
LiCo _{0.5} Ni _{0.5} O ₂	5.6	0.64	20	2.06	—
LiMn _{0.5} Ni _{0.5} O ₂	11	1.76	24	3.10	—

In conclusion, it seems that the extrapolated $G_0W_0@PBE$ band gaps are in reasonable agreement to experimental data and also work considerably well for all layered TM oxides under study (except $\text{LiCo}_{0.5}\text{Mn}_{0.5}\text{O}_2$ due to the aforementioned changes in the electronic structure with α). However, it must be mentioned that the seemingly good agreement to experimental band gaps might be due to error cancellation as direct comparisons to experiment are not completely fair. The calculations yield 0 K band gaps while the experimental values were obtained at finite temperatures. Moreover, the model used in the simulations of stoichiometric LiNiO_2 might not represent the experimental structure exactly which has been observed to be nonstoichiometric, as discussed in the method part. This can also accidentally improve the agreement to experiment.

Using these extrapolated $G_0W_0@PBE$ band gaps to determine the corresponding optimal HF-mixing parameters ($\alpha^{\text{ext.}}$) for PBE0 is straight forward due to the linear trend of band gap versus α . The corresponding optimal $\alpha^{\text{ext.}}$ values are shown in Table I along with their band gaps and are also visualized in Fig. 2. For $\text{LiCo}_{0.5}\text{Mn}_{0.5}\text{O}_2$ no mixing parameter could be determined because of the irregular behavior of electronic structure and α explained in the previous section.

The optimal mixing parameters vary within a range of roughly 5% which is relatively large as a change in band gap of up to 0.75 eV can arise for these compounds from this variation. The optimal $\alpha^{\text{ext.}}$ for the binary systems cannot be extrapolated as mean value of the corresponding pure materials independent if the charges of the individual species change from the pure and binary system ($\text{LiMn}_{0.5}\text{Ni}_{0.5}\text{O}_2$) or not ($\text{LiCo}_{0.5}\text{Ni}_{0.5}\text{O}_2$). Therefore the optimal mixing parameter seems to be system-dependend and using the mean value over all compositions of approximately 8.5% appears to be the efficient trade off for all compositions. This HF mixing is significantly lower than the default value of 25% but in agreement with other studies on similar (layered) TM oxides that rely directly or indirectly on experimental properties and also suggested significantly lower HF mixing-parameters for hybrid functionals [6,14,35].

The corrections in the band gap G_0W_0 is introducing to the PBE0 starting point, namely the differences in each point of Fig. 2 and the upper plot in Fig. 5, are visualized in the lower plot of Fig. 5. In general, a pronounced increase of the band gap by G_0W_0 to the PBE0 starting point (positive correction) is observed for small α that gets smaller for higher α and even turns into a decrease (negative correction) for high α . This behavior can be utilized to define a different optimal HF mixing α^{GW} for each compound at the point where the PBE0 starting band gap is not altered by a consecutive G_0W_0 calculation (correction is zero in lower plot of Fig. 5). It should be noted that this α^{GW} fitting-approach was also proposed by Chen *et al.* [38]. In agreement to their study, we also find that the determined optimal α^{GW} values using this zero-correction approach are higher than those agreeing better to experimental values (e.g., aforementioned $\alpha^{\text{ext.}}$). It should be mentioned that the seemingly worse agreement to the experimental band gaps of the higher level of theory approach (α^{GW}) compared to the extrapolated $G_0W_0@PBE$ approach might be due to error cancellations in the latter approach or fundamental differences of experiment and calculation (e.g., temperature, model/structure) as discussed above. Such error cancellations were also discussed in the work of Wiktor *et al.* [78] where $G_0W_0@PBE$ delivered the best agreement to experimental values for perovskites of the type CsPbX ($X = \text{Cl, Br, and I}$), even better than fully self-consistent (in eigenvalues and wave functions) GW calculations with vertex correction. The authors also showed that when accounting for effects such as temperature and spin-orbit coupling the higher level method is again in better agreement with experiment and concluded that without these corrections $G_0W_0@PBE$ showed better agreement to experimental band gaps because of error cancellations. A similar cancellation could also be present in the extrapolated $G_0W_0@PBE$ approach for the materials in this work.

The optimal α^{GW} along with their corresponding band gaps for the studied layered TM oxides in this work are shown in Table I and are visualized in Fig. 2. Interestingly, these values and especially the mean value of 22% are close to the default value of 25% that has been derived by perturbation theory approaches [33] as well as the value of 19% obtained by xc kernel analysis in a very recent study [79]. Therefore values of 20% to 25% appear to have a strong theoretical foundation in general and also for layered TM oxides. It is worth mentioning that the optimal α^{GW} of the binary systems seems to be predictable as mean values of the α^{GW} of the pure materials. For example, LiCoO_2 and LiNiO_2 both have an optimal α^{GW} value of 20% and so does their binary mixture ($\text{LiMn}_{0.5}\text{Ni}_{0.5}\text{O}_2$) has a value of 20% as well. $\text{LiMn}_{0.5}\text{Ni}_{0.5}\text{O}_2$ shows an optimal mixing α^{GW} of 24% which is exactly the mean value of the pure materials, 20% (LiNiO_2) and 28% (LiMnO_2), respectively. Moreover, this predictive behavior was also verified for the ternary system ($\text{Co:Mn:Ni} = 1:1:1$) of species under study that showed an optimal α^{GW} of 22.5% which is essentially the sum of the optimal α^{GW} parameters of the pure compounds weighted by their concentration in the ternary system. This linear dependence of optimal α^{GW} on the concentrations of constituting elements is different to optimal $\alpha^{\text{ext.}}$ where no trend was

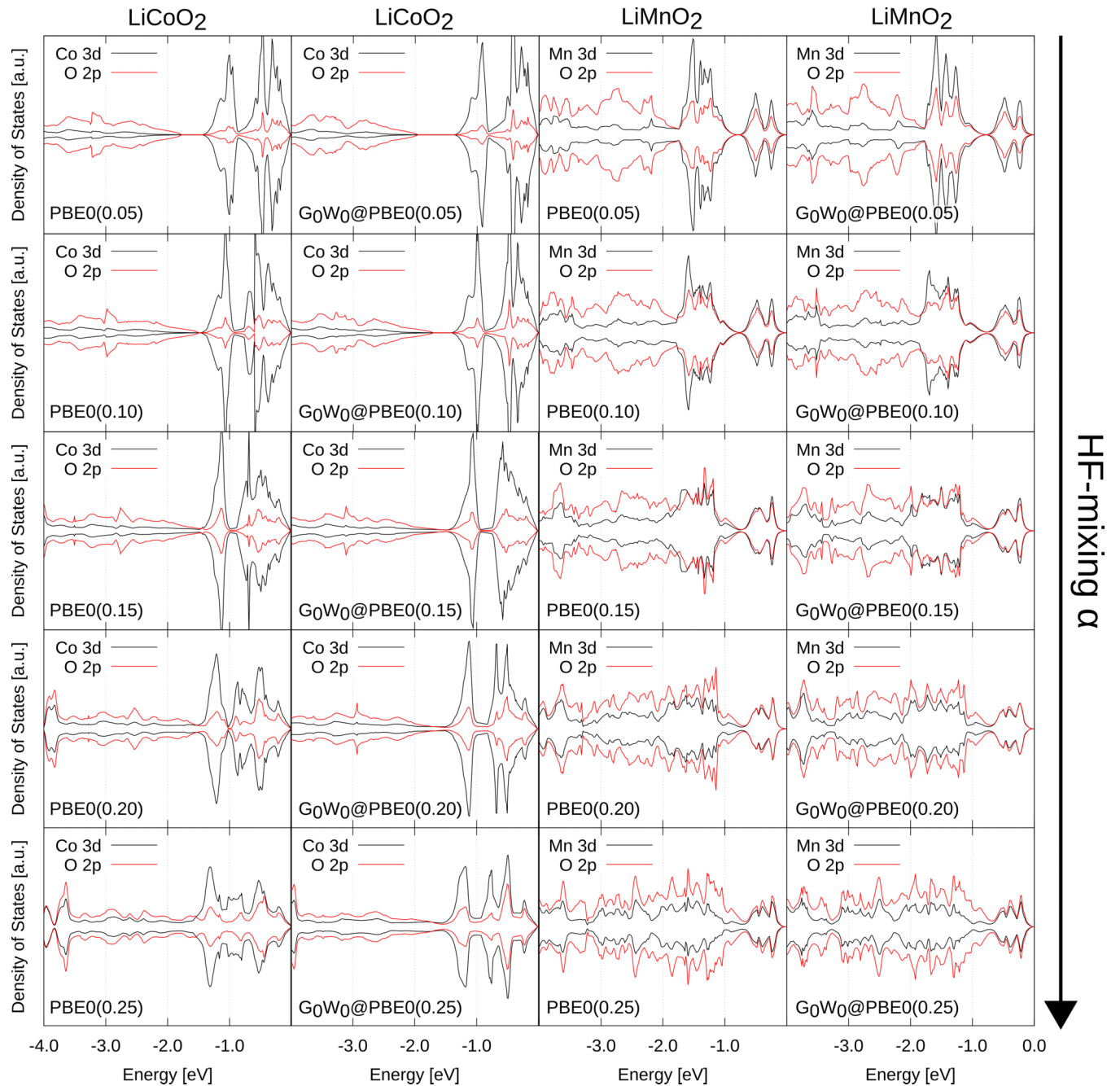


FIG. 6. pDOS of O 2p orbitals (red) and TM 3d orbitals (black) for LiCoO₂ (first column) and LiMnO₂ (third column) at increasing HF mixing (top to bottom) along with the pDOS obtained from a consecutive G_0W_0 step (second and fourth column).

observed but allows to immediately predict α^{GW} for mixed compounds.

Regarding the computed DOS below the Fermi energy, it can be concluded that no significant change by the consecutive G_0W_0 step is observed and almost the same features as in the PBE0 starting points (Fig. 6) appear. Consequently, also the same trends in terms of hybridization of O 2p orbitals and Co/Mn 3d orbitals as discussed for Fig. 4 in the previous section can be observed proving again that hybrids are a rather advanced starting point for GW calculations.

C. Fully self-consistent GW calculations at different PBE0 HF mixing parameters and influence of screening the HF part

To further verify the obtained trends within the G_0W_0 approach, a higher level of GW was also employed where eigenvalues were iterated to self-consistency in G and W (sometimes also denoted as “ev GW ”) for LiCoO₂ and LiNiO₂. In general, it is expected that this approach has a tendency to over-predict band gaps due to missing vertex corrections [58]. A tendency towards larger band gaps is also observed for the layered TM oxides in this study (cf. Fig. 7). However,

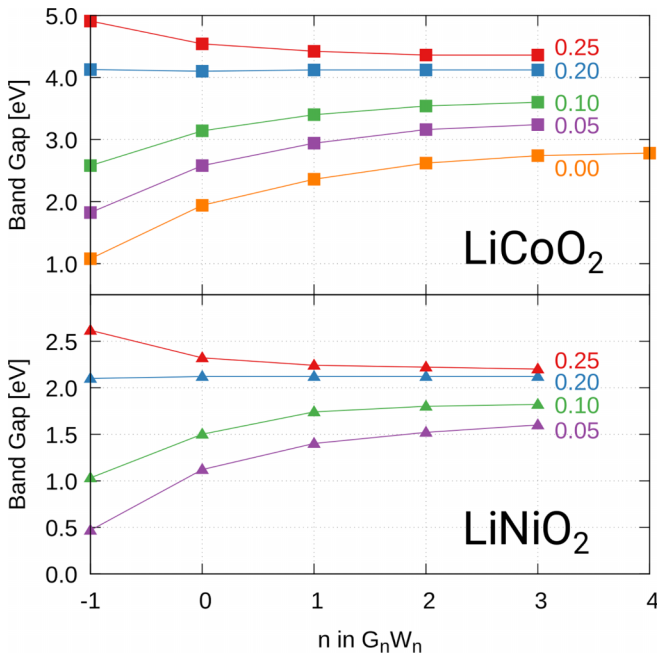


FIG. 7. Band gaps of iterations (n) of fully self-consistent GW calculations with different PBE0 starting points for LiCoO₂ (top) and LiNiO₂ (bottom). Iteration $n = -1$ corresponds to the PBE0 band gap and $n = 0$ to the G_0W_0 band gap.

an excellent agreement with the experimental value of 2.7 eV [75] is found for LiCoO₂ by applying fully self-consistent GW at a PBE starting point. Overall, the calculated band gaps get closer to their corresponding converged values with increasing the number of GW iterations but the self-consistent results still maintain (strongly) starting point dependent as also found in another study on a different TM oxide and can be related to different starting wave functions [57,58].

For LiCoO₂ and LiNiO₂, the converged GW band gaps become larger with higher HF mixing in the starting point, are lowered by GW for mixings above 20% (the determined optimal α^{GW} in the previous section), and increased for lower mixing values. The results also show that the number of steps to converge the band gaps strongly varies with the HF mixing in the starting point and is larger the more different the initial mixing parameter is from the optimal mixing-parameter α^{GW} . In fact, optimal α^{GW} (20%) that were obtained in the previous section do not show a significant change in band gap over all performed GW steps proving that this approach of determining the optimal α^{GW} delivers direct access to fully self-consistent GW band gaps at the computational cost of a hybrid functional. That the optimal α^{GW} mixing parameters are not just consistent in G_0W_0 but also in GW underlines their strong theoretical foundation.

Lastly, also the effect of applying range-separated hybrid functionals with screening in the HF part (HSE approach) compared to the unscreened PBE0 functional was investigated as this approximation can offer some computational benefits [40]. The two inverse screening length of $\omega = 0.3 \text{ \AA}^{-1}$ (HSE03) [40] and $\omega = 0.2 \text{ \AA}^{-1}$ (HSE06) [41] were employed and the results were compared to those with PBE0. Their dependence of the band gap and the HF mixing-parameter is

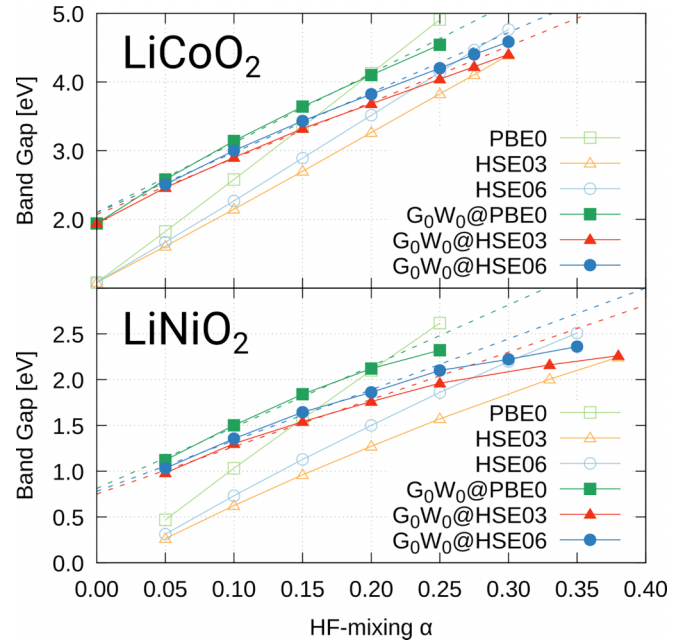


FIG. 8. G_0W_0 and hybrid functional band gaps for LiCoO₂ (top) and LiNiO₂ (bottom) for hybrid functional starting points with different mixing parameters and different screenings of the HF part (HSE06, HSE03). The linear functions for the extrapolated G_0W_0 @PBE band gaps are indicated by the dashed lines.

plotted in Fig. 8, indicating an almost perfectly linear trend (minor deviations for LiNiO₂ with HSE at high mixing and screening parameters) as observed for PBE0 in this study as well as in other studies with HSE functionals [6,80].

HSE06 band gaps are slightly higher but in fair agreement with the computational HSE06 study of Seo *et al.* [6] for LiCoO₂ and LiNiO₂. In agreement with the studies of Komsa *et al.* [80], the slopes of linear fits become smaller with higher ω and consequently higher HF mixing-parameters are required to obtain the same band gaps compared to PBE0. Applying G_0W_0 to the HSE starting points also yields deviations from the linear trend as for PBE0 resulting in a crossing point of both approaches that allows for the determination of an optimal α^{GW} . At this α , G_0W_0 (and as discussed above also higher levels of GW) causes no correction to the band gap of the bare hybrid functional (cf. Fig. 8). The corresponding optimal mixing parameters α^{GW} are 25% (LiCoO₂-HSE06), 30% (LiNiO₂-HSE06), 30% (LiCoO₂-HSE03), and 38% (LiNiO₂-HSE03). For HSE03 the parameters are higher than the default of 25%, while for HSE06 both values are fairly close to 25%. This proves the superior fitting of the screening parameter in HSE06 over HSE03 for the investigated layered TM oxides as the mixing parameter was fixed to 25% in HSE, while technically both, the mixing parameter and the screening parameter could be fitted (to some extent) to obtain the same result [41,81]. This shows that the default HF mixing within the HSE06 functional can be reasoned quite well by the α^{GW} fitting-approach for the layered TM oxides. However, in contrast to the PBE0 case the optimal α^{GW} mixing parameter becomes composition-dependent for LiCoO₂ and LiNiO₂ when screening is introduced. The

flatter slope that comes along with higher screening has the beneficial effect that the band gaps become less sensitive to the HF mixing. Even though the determined LiNiO_2 -HSE06 optimal mixing parameter α^{GW} is with 30% slightly higher than the default, the pure hybrid band gap and the corresponding G_0W_0 solution are already relatively close at 25% (cf. Fig. 8).

Note that computed band gaps using the optimal α^{GW} values corresponding to each screening are almost the same for all functionals (PBE0, HSE03, HSE06) with a small drift towards higher values at higher ω . This proves that the determined band gaps using $\alpha^{GW}(\omega)$ show a high consistency across several high-level theory methods constituting them as promising candidates for describing layered TM oxides. Although the $\alpha^{GW}(\omega)$ over-predicts the experimental band gaps of the materials under study, it is reasonably close to the default mixing values of the functionals as mentioned above.

The screened hybrids also allow for the extrapolated $G_0W_0@PBE$ approach which showed better agreement to experimental band gaps for PBE0 in the previous section. As this approach tries to extrapolate to PBE level, using HSE functionals should not alter the extrapolated band gaps as the differences to PBE0 are just in the HF part that should be eliminated by the extrapolation. Indeed, the linear fits in Fig. 8 (dashed lines) show the same extrapolated $G_0W_0@PBE$ band gaps for all functionals within an accuracy way below 0.1 eV. This proves that extrapolating the trends of the G_0W_0 band gaps by a linear function in the intermediate α range of 5%–20% is reasonable for the layered TM oxides in this study. Moreover, the usage of screened hybrids can slightly reduce the enormous computational effort of this approach as they offer a computational performance advantage over PBE0 [40]. Applying extrapolation, optimal mixing parameters $\alpha^{ext.}$ of 8.5% (LiCoO_2 -HSE06), 11% (LiNiO_2 -HSE06), 9.2% (LiCoO_2 -HSE03), and 12% (LiNiO_2 -HSE03) can be determined. Compared to PBE0, the optimal $\alpha^{ext.}$ are higher because the band gaps are the same but the slopes of the linear trends of the band gap and α become smaller for higher screenings as mentioned above. The robustness of extrapolated $G_0W_0@PBE$ towards different hybrid functionals based on PBE along with the reasonable agreement to experimental results is quite encouraging for the idea of extrapolating band gaps from descriptions with wave functions and alignment of states more close to GW , namely, hybrid functionals. This approach can be utilized to determine *ab initio* band gaps in layered TM oxides close to experimental values.

IV. SUMMARY AND CONCLUSION

We presented two different nonempirical fitting approaches to determine the HF mixing parameter in PBE-based hybrids to calculate electronic structures of layered TM oxides. While one approach yields satisfactory agreement to experiment for LiCoO_2 and LiNiO_2 , the other, despite its stronger theory foundation, overpredicts band gaps of LiCoO_2 and LiNiO_2 compared to experimental values significantly. The first approach suggests low optimal mixing parameters of $\alpha^{ext.} \approx 8.5\%$ and the second fitting approach yields optimal mixing of

$\alpha^{GW} \approx 22\%$ which is in fair agreement to default mixing of 25% employed in hybrid functionals such as PBE0, HSE03, and HSE06. We defined the first fitting approach by extrapolation of G_0W_0 band gaps to $G_0W_0@PBE$ band gaps using $G_0W_0@PBE0$ band gaps with intermediate mixing parameters in the range of 5%–20%. We also showed that almost same extrapolated $G_0W_0@PBE$ band gaps can be fitted from G_0W_0 calculations at screened PBE-based hybrid functionals (HSE). However, for these screened hybrids, the corresponding optimal mixing increases with the screening parameter. For the second fitting approach, the HF mixing that directly yields the band gap of a consecutive G_0W_0 calculation was chosen. It was proven that this mixing parameter is also valid at fully self-consistent GW , allowing access to accurate GW band gaps at the much lower computational cost of hybrid functionals. For screened hybrid functionals, we found strong variation in optimal mixing $\alpha^{GW}(\omega)$ depending on screening ω but only minor changes in the corresponding computed band gap. Moreover, dependence of optimal mixing α^{GW} and concentration of elements in the studied composition shows linearity, allowing for the prediction of optimal HF mixing.

It is encouraging that (extrapolated) $G_0W_0@PBE$ appears to obtain band gaps from purely computational methods that are in reasonable agreement with experiment and also that the default mixing of 25% is justified not just by perturbation theory but also high level GW calculations. Further works, however, are required to understand the large discrepancy between the optimal $\alpha^{ext.}$ (close to experimental band gap) and α^{GW} (strong theory foundation) HF mixing-parameters in hybrids that was shown by the two different nonempirical GW fitting approaches in this work as well as if the better agreement to experiment of the lower level of theory approach ($\alpha^{ext.}$) might be caused by error cancellations.

ACKNOWLEDGMENTS

The authors gratefully acknowledge funding from the “Deutsche Forschungsgemeinschaft” (DFG, German Research Foundation) under project No. 501562980 and the computing time granted through JARA-HPC on the supercomputer JURECA [82] at Forschungszentrum Jülich under Grant No. jiek12.

APPENDIX

TABLE II. Fitted linear functions of the form $BG(\alpha) = a \times \alpha + b$ of the PBE0 band gaps (BG) as function of the HF mixing parameter α .

Compound	a (eV)	b (eV)
LiCoO_2	15.436 ± 0.062	1.042 ± 0.010
LiMnO_2	12.054 ± 0.126	1.399 ± 0.021
LiNiO_2	10.732 ± 0.105	-0.052 ± 0.017
$\text{LiCo}_{0.5}\text{Mn}_{0.5}\text{O}_2$	11.136 ± 2.651	-0.672 ± 0.440
$\text{LiCo}_{0.5}\text{Ni}_{0.5}\text{O}_2$	9.820 ± 0.045	0.094 ± 0.007
$\text{LiMn}_{0.5}\text{Ni}_{0.5}\text{O}_2$	10.440 ± 0.168	0.599 ± 0.028

TABLE III. Calculated unpaired electrons (UPE) for the ions in the studied compounds and charges estimated from UPE assuming octahedral ligand-field splitting of d orbitals at 25% HF mixing. As discussed in the text, average UPE/charges over all ions of one species are given for $\text{LiCo}_{0.5}\text{Mn}_{0.5}\text{O}_2$

Compound	UPE			Charges		
	Co	Mn	Ni	Co	Mn	Ni
LiCoO_2	0.0	—	—	3	—	—
LiMnO_2	—	3.7	—	—	3	—
LiNiO_2	—	—	0.9	—	—	3
$\text{LiCo}_{0.5}\text{Mn}_{0.5}\text{O}_2$	0.4	2.3	—	2.7	3.3	—
$\text{LiCo}_{0.5}\text{Ni}_{0.5}\text{O}_2$	0.0	—	0.9	3	—	3
$\text{LiMn}_{0.5}\text{Ni}_{0.5}\text{O}_2$	—	3.0	1.6	—	4	2

TABLE IV. Parameters of the linear fits ($f(\alpha) = a \times \alpha + b$) for G_0W_0 @PBE0 band gaps against different PBE0 HF mixing parameters α in the range of 5% to 20%. The y intercepts b correspond to the discussed extrapolated G_0W_0 @PBE band gaps.

Compound	a (eV)	b (eV)
LiCoO_2	10.128 ± 0.317	2.101 ± 0.043
LiMnO_2	7.440 ± 0.259	2.831 ± 0.036
LiNiO_2	6.680 ± 0.318	0.811 ± 0.043
$\text{LiCo}_{0.5}\text{Mn}_{0.5}\text{O}_2$	13.086 ± 3.161	-0.891 ± 0.433
$\text{LiCo}_{0.5}\text{Ni}_{0.5}\text{O}_2$	7.246 ± 0.578	0.640 ± 0.079
$\text{LiMn}_{0.5}\text{Ni}_{0.5}\text{O}_2$	6.086 ± 0.522	1.760 ± 0.071

- [1] L. Wang, T. Maxisch, and G. Ceder, *Phys. Rev. B* **73**, 195107 (2006).
- [2] S. Lany, *Phys. Rev. B* **87**, 085112 (2013).
- [3] U. Diebold, J. F. Anderson, K.-O. Ng, and D. Vanderbilt, *Phys. Rev. Lett.* **77**, 1322 (1996).
- [4] R. Sakuma and F. Aryasetiawan, *Phys. Rev. B* **87**, 165118 (2013).
- [5] J. Graetz, C. C. Ahn, H. Ouyang, P. Rez, and B. Fultz, *Phys. Rev. B* **69**, 235103 (2004).
- [6] D.-H. Seo, A. Urban, and G. Ceder, *Phys. Rev. B* **92**, 115118 (2015).
- [7] S.-T. Myung, F. Maglia, K.-J. Park, C. S. Yoon, P. Lamp, S.-J. Kim, and Y.-K. Sun, *ACS Energy Lett.* **2**, 196 (2017).
- [8] P. Wang, Y. You, Y. Yin, and Y. Guo, *Adv. Energy Mater.* **8**, 1701912 (2018).
- [9] K. Mizushima, P. Jones, P. Wiseman, and J. Goodenough, *Mater. Res. Bull.* **15**, 783 (1980).
- [10] Y. Nishi, *Interf. Mag.* **25**, 71 (2016).
- [11] T. Ohzuku, A. Ueda, and M. Nagayama, *J. Electrochem. Soc.* **140**, 1862 (1993).
- [12] A. R. Armstrong and P. G. Bruce, *Nature (London)* **381**, 499 (1996).
- [13] A. Chakraborty, S. Kunnikuruvan, S. Kumar, B. Markovsky, D. Aurbach, M. Dixit, and D. T. Major, *Chem. Mater.* **32**, 915 (2020).
- [14] V. Singh, M. Kosa, K. Majhi, and D. T. Major, *J. Chem. Theory Comput.* **11**, 64 (2015).
- [15] A. R. Genreith-Schriever, H. Banerjee, A. S. Menon, E. N. Bassey, L. F. Piper, C. P. Grey, and A. J. Morris, *Joule* **7**, 1623 (2023).
- [16] F. Iori, M. Gatti, and A. Rubio, *Phys. Rev. B* **85**, 115129 (2012).
- [17] M. E. Lines, *Phys. Rev. B* **43**, 11978 (1991).
- [18] H. Peng and S. Lany, *Phys. Rev. B* **85**, 201202(R) (2012).
- [19] C. Rodl, F. Fuchs, J. Furthmuller, and F. Bechstedt, *Phys. Rev. B* **79**, 235114 (2009).
- [20] M. Jain, J. R. Chelikowsky, and S. G. Louie, *Phys. Rev. Lett.* **107**, 216806 (2011).
- [21] A. D. Becke, *J. Chem. Phys.* **98**, 1372 (1993).
- [22] M. Eckhoff, P. E. Blochl, and J. Behler, *Phys. Rev. B* **101**, 205113 (2020).
- [23] V. L. Chevrier, S. P. Ong, R. Armiento, M. K. Y. Chan, and G. Ceder, *Phys. Rev. B* **82**, 075122 (2010).
- [24] C. Franchini, V. Bayer, R. Podloucky, J. Paier, and G. Kresse, *Phys. Rev. B* **72**, 045132 (2005).
- [25] C. Franchini, R. Podloucky, J. Paier, M. Marsman, and G. Kresse, *Phys. Rev. B* **75**, 195128 (2007).
- [26] J. Wrobel, K. J. Kurzydowski, K. Hummer, G. Kresse, and J. Piechota, *Phys. Rev. B* **80**, 155124 (2009).
- [27] V. I. Anisimov, J. Zaanen, and O. K. Andersen, *Phys. Rev. B* **44**, 943 (1991).
- [28] L. Vaugier, H. Jiang, and S. Biermann, *Phys. Rev. B* **86**, 165105 (2012).
- [29] F. Zhou, M. Cococcioni, C. A. Marianetti, D. Morgan, and G. Ceder, *Phys. Rev. B* **70**, 235121 (2004).
- [30] L. I. Bendavid and E. A. Carter, *First Principles Approaches to Spectroscopic Properties of Complex Materials* (Springer, Berlin, Heidelberg, 2014), pp. 47–98.
- [31] B. Himmetoglu, A. Floris, S. de Gironcoli, and M. Cococcioni, *Int. J. Quantum Chem.* **114**, 14 (2014).
- [32] A. D. Becke, *J. Chem. Phys.* **104**, 1040 (1996).
- [33] J. P. Perdew, M. Ernzerhof, and K. Burke, *J. Chem. Phys.* **105**, 9982 (1996).
- [34] P. Cortona, *J. Chem. Phys.* **136**, 086101 (2012).
- [35] R. A. House, G. J. Rees, K. McColl, J.-J. Marie, M. Garcia-Fernandez, A. Nag, K.-J. Zhou, S. Cassidy, B. J. Morgan, M. Saiful Islam, and P. G. Bruce, *Nat. Energy* **8**, 351 (2023).
- [36] X. Feng and N. M. Harrison, *Phys. Rev. B* **70**, 092402 (2004).
- [37] W. Chen and A. Pasquarello, *Phys. Rev. B* **96**, 020101(R) (2017).
- [38] W. Chen and A. Pasquarello, *Phys. Rev. B* **90**, 165133 (2014).
- [39] M. Sotoudeh, S. Rajpurohit, P. Blochl, D. Mierwaldt, J. Norpoth, V. Roddatis, S. Mildner, B. Kressdorf, B. Iffland, and C. Jooss, *Phys. Rev. B* **95**, 235150 (2017).
- [40] J. Heyd, G. E. Scuseria, and M. Ernzerhof, *J. Chem. Phys.* **118**, 8207 (2003).
- [41] A. V. Krukau, O. A. Vydrov, A. F. Izmaylov, and G. E. Scuseria, *J. Chem. Phys.* **125**, 224106 (2006).

- [42] J. H. Skone, M. Govoni, and G. Galli, *Phys. Rev. B* **89**, 195112 (2014).
- [43] L. Kronik, T. Stein, S. Refaely-Abramson, and R. Baer, *J. Chem. Theory Comput.* **8**, 1515 (2012).
- [44] S. Refaely-Abramson, M. Jain, S. Sharifzadeh, J. B. Neaton, and L. Kronik, *Phys. Rev. B* **92**, 081204(R) (2015).
- [45] G. Miceli, W. Chen, I. Reshetnyak, and A. Pasquarello, *Phys. Rev. B* **97**, 121112(R) (2018).
- [46] E. Wruss, E. Zojer, and O. T. Hofmann, *J. Phys. Chem. C* **122**, 14640 (2018).
- [47] I. P. R. Moreira, F. Illas, and R. L. Martin, *Phys. Rev. B* **65**, 155102 (2002).
- [48] D.-H. Seo, J. Lee, A. Urban, R. Malik, S. Kang, and G. Ceder, *Nat. Chem.* **8**, 692 (2016).
- [49] A. Konarov, H. J. Kim, J. Jo, N. Voronina, Y. Lee, Z. Bakenov, J. Kim, and S. Myung, *Adv. Energy Mater.* **10**, 2001111 (2020).
- [50] M. S. Hybertsen and S. G. Louie, *Phys. Rev. B* **34**, 5390 (1986).
- [51] M. Shishkin and G. Kresse, *Phys. Rev. B* **75**, 235102 (2007).
- [52] M. Gerosa, C. E. Bottani, L. Caramella, G. Onida, C. Di Valentin, and G. Pacchioni, *Phys. Rev. B* **91**, 155201 (2015).
- [53] M. Shishkin and G. Kresse, *Phys. Rev. B* **74**, 035101 (2006).
- [54] H. Jiang, R. I. Gomez-Abal, P. Rinke, and M. Scheffler, *Phys. Rev. B* **82**, 045108 (2010).
- [55] J. Klimes, M. Kaltak, and G. Kresse, *Phys. Rev. B* **90**, 075125 (2014).
- [56] M. J. Han, H. Kino, and T. Kotani, *Phys. Rev. B* **90**, 035127 (2014).
- [57] P. Liao and E. A. Carter, *Phys. Chem. Chem. Phys.* **13**, 15189 (2011).
- [58] F. Fuchs, J. Furthmüller, F. Bechstedt, M. Shishkin, and G. Kresse, *Phys. Rev. B* **76**, 115109 (2007).
- [59] P. E. Blöchl, *Phys. Rev. B* **50**, 17953 (1994).
- [60] G. Kresse and J. Furthmüller, *Phys. Rev. B* **54**, 11169 (1996).
- [61] J. Sugiyama, Y. Ikedo, K. Mukai, H. Nozaki, M. Mansson, O. Ofer, M. Harada, K. Kamazawa, Y. Miyake, J. H. Brewer, E. J. Ansaldo, K. H. Chow, I. Watanabe, and T. Ohzuku, *Phys. Rev. B* **82**, 224412 (2010).
- [62] C. Delmas, C. Fouassier, and P. Hagenmüller, *Physica B+C* **99**, 81 (1980).
- [63] Z. Chen, H. Zou, X. Zhu, J. Zou, and J. Cao, *J. Solid State Chem.* **184**, 1784 (2011).
- [64] J. P. Perdew, K. Burke, and M. Ernzerhof, *Phys. Rev. Lett.* **77**, 3865 (1996).
- [65] J. Heyd and G. E. Scuseria, *J. Chem. Phys.* **120**, 7274 (2004).
- [66] K. Momma and F. Izumi, *J. Appl. Cryst.* **41**, 653 (2008).
- [67] V. Wang, N. Xu, J.-C. Liu, G. Tang, and W.-T. Geng, *Comput. Phys. Commun.* **267**, 108033 (2021).
- [68] C. A. Marianetti, D. Morgan, and G. Ceder, *Phys. Rev. B* **63**, 224304 (2001).
- [69] D. J. Singh, *Phys. Rev. B* **55**, 309 (1997).
- [70] X. Cai, S.-H. Wei, P. Deak, C. Franchini, S.-S. Li, and H.-X. Deng, *Phys. Rev. B* **108**, 075137 (2023).
- [71] D. Koller, P. Blaha, and F. Tran, *J. Phys.: Condens. Matter* **25**, 435503 (2013).
- [72] F. Vines, O. Lamiel-Garcia, K. Chul Ko, J. Yong Lee, and F. Illas, *J. Comput. Chem.* **38**, 781 (2017).
- [73] I. B. Slima, K. Karoui, and A. B. Rhaïem, *Ionics* **29**, 1731 (2023).
- [74] K. Kushida and K. Kuriyama, *Solid State Commun.* **123**, 349 (2002).
- [75] J. van Elp, J. L. Wieland, H. Eskes, P. Kuiper, G. A. Sawatzky, F. M. F. de Groot, and T. S. Turner, *Phys. Rev. B* **44**, 6090 (1991).
- [76] N. Nath Shukla and R. Prasad, *J. Phys. Chem. Solids* **67**, 1731 (2006).
- [77] F. Kong, R. C. Longo, M.-S. Park, J. Yoon, D.-H. Yeon, J.-H. Park, W.-H. Wang, S. KC, S.-G. Doo, and K. Cho, *J. Mater. Chem. A* **3**, 8489 (2015).
- [78] J. Wiktor, U. Rothlisberger, and A. Pasquarello, *J. Phys. Chem. Lett.* **8**, 5507 (2017).
- [79] Z. A. Moldabekov, M. Lokamani, J. Vorberger, A. Cangì, and T. Dornheim, *J. Phys. Chem. Lett.* **14**, 1326 (2023).
- [80] H.-P. Komsa, P. Broqvist, and A. Pasquarello, *Phys. Rev. B* **81**, 205118 (2010).
- [81] J. E. Moussa, P. A. Schultz, and J. R. Chelikowsky, *J. Chem. Phys.* **136**, 204117 (2012).
- [82] P. Thörnig, *J. Large-Scale Res. Facil.* **7**, A182 (2021).